energies

MDPI

Article

A Steady State Model for Burning Coal Mine Methane in a Reverse Flow Burner

Jinsheng Lv, Junrui Shi *, Mingming Mao, Xiangjin Kong and Dan Zhou

School of Transportation and Vehicle Engineering, Shandong University of Technology, Zibo 255049, China; lvjinsheng@sdut.edu.cn (J.L.); maomingming@sdut.edu.cn (M.M.); kongxiangjin@sdut.edu.cn (X.K.); zhoudan@sdut.edu.cn (D.Z.)

* Correspondence: shijunrui@sdut.edu.cn; Tel.: +86-0553-278-4453

Abstract: In this study, a steady state model for burning of coal mine methane in a Reverse Flow Burner (RFB) with full kinetics was developed by analogy of a steady counter-flow reactor, and the developed model was used for quick prediction of the lean combustibility limit (LCL). The model was successfully validated with experimental and numerical results, and it was shown that the developed model has excellent accuracy and computational efficiency. Good agreement between the predicted temperature, LCL, and the experiments was observed. The LCL of the equivalence ratio of 0.022 for methane/air mixture was obtained by the developed model. The model was then used to evaluate LCL for the RFB, focusing on the effect of heat loss and burner length on LCL. This indicated that the computational time using the developed model can be reduced by a factor of 1560 compared to the complete transient model.

Keywords: Reverse Flow Burner; steady state model; lean combustibility limit; thermal oxidation; numerical simulation

Citation: Lv, J.; Shi, J.; Mao, M.; Kong, X.; Zhou, D. A Steady State Model for Burning Coal Mine Methane in a Reverse Flow Burner. *Energies* **2021**, *14*, 7957. https://doi.org/10.3390/en14237957

Academic Editor: Aiwu Fan

Received: 28 October 2021
Accepted: 23 November 2021
Published: 29 November 2021

1. Introduction

Filtration combustion has attracted much attention due to the enhanced mass and heat transfer process in porous media. As a result, superadiabatic combustion may take place in the reactor; low heating-value gas can be burned and heat recovery from these gases can be realized. The forced ventilation process in coal mining emits considerable methane. In 2009, the global Ventilation Air Methane (VAM) was about 14 billion m^3. There are three gas streams containing methane from coal—gas drained from the coal seam before mining (60–95%, vol% CH_4), from work zones of the mine (30–95%, vol% CH_4) and by ventilation air (0.1–1.0%, vol% CH_4) [1,2].

Because of the pressure derived from the need to burn coal mine methane and lower emissions in combustion of low heat content gas, new combustion technologies and devices are sought. Of these technologies, superadiabatic combustion has been proven to be an effective way to extend lean combustibility limits (LCLs) and control pollutant emissions compared to conventional combustion [3].

The concept of superadiabatic or excess enthalpy combustion was introduced by Egerton [4] and Weinberg [5]. Since then, superadiabatic combustion in a packing bed has been investigated intensively by experimental [6–8], theoretical [9–11], and numerical studies [12–14]. One of the most severe problems for superadiabatic combustion is the extension of the LCL. It is also important for the burner to be able to minimize CO and NOx emissions.

The early experimental studies focused on the extending the LCL of a porous burner with unidirectional flow. Zhdanok et al. [6] studied the superadiabatic combustion in a packed bed with alumina pellets for methane/air mixture, and proposed the idea of overlapping the thermal wave and combustion wave to obtain superadiabatic combustion. It was confirmed experimentally that the combustion temperature in the packed bed

was about 2.8 times the normal adiabatic temperature, and the LCL was extended to the equivalence ratio of 0.15. Furthermore, an analytical solution of the relationship between flame temperature, and thermal and combustion wave speed, was presented. The superadiabatic combustion mechanism through the overlapping thermal and combustion wave was validated theoretically by Shi et al. [10]; an analytical solution of the temperatures in the packed bed was presented, which was divided into the initial temperature field and the influence of the reaction heat.

To further extend the LCL, an RFB was proposed by the researchers, in which the flow direction of fuel/air mixture was periodically switched within a certain time interval. As a result, solid heat stored in the downstream in the previous half cycle was used to preheat the fresh mixture. Thus, the LCL could be extended and the combustion was stabilized in the porous burner. Experimental studies on superadiabatic combustion in the RFB have been extensively conducted by researchers. Hoffmann et al. [15] reported that the LCL was extended to the equivalence ratio of 0.026. Heat recovered from coal mine methane via an RFB with embedded heat exchangers has also been extensively studied [15–17]. Gosiewski et al. [1] reported that an RFB system can be stable when the concentration of coal mine methane is greater than 0.2% vol.% and heat recovery from the products may be obtained when methane concentration is higher than 0.4 vol.%.

Porous media combustion technology provides many benefits, but also leads to difficulties for simulations due to multiple time and length scales [18]. The volume-averaged method and local simulation are the two main approaches used in the numerical studies. To simplify the modeling, the volume-averaged method with one-step kinetics has been widely used [18–23]. Hanamura et al. [19] numerically investigated superadiabatic combustion in an RFB using a one-dimensional two-temperature model with global chemical kinetics. It was shown that the flame temperature in the burner was 13 times greater than the conventional one. Dobrego et al. [20] conducted theoretical and numerical studies on the LCL in an RFB using one-step kinetics. Bubnovich et al. [21] carried out simulations on the influence of particle diameter on the stabilization operation region using a 1D transient model with global chemical kinetics. They found that the increase in the particle diameter leads to an increase in the stabilization zone under the condition with and without heat extraction.

Premixed gas combustion in porous media with a homogeneous structure is transient combustion, and simulations with the transient model and full chemical kinetics are extremely time consuming. It is known that more than 40–60 half cycles are required for an RFB to reach a quasi-steady condition. The predictions by Bubnovich et al. [21] showed that stationary temperature profiles were reached within 2000 s with a time step of 0.01 s under the conditions of the equivalence ratio of 0.25 and mixture velocity of 0.25 m/s. Yakovlev et al. [13] adopted a multi-scale method to speed up calculations of filtration combustion using a local simulation with full chemical kinetics; 8×10^{-5} s was used for the gas phase equation and 0.05 s for the solid phase equation. Vourliotakis et al. [23] reported that more than a week of Central Processing Unit (CPU) time was needed for 3D CFD simulation of syngas prediction in porous media using GRI-Mech 3.0 for only one case of computation. It is obvious that tremendous computational time and resources are required to simulate transient combustion with full kinetics.

To speed up the computation of chemistry and save computational time, four different approaches were found in the previous studies on filtration combustion, namely, reduction in the computational domain; using simplified chemical kinetics; speeding up the chemistry; and the multi-scale method. Reduction in the computational domain by symmetry conditions or selecting the representational part of the burner has been widely used by researchers [24]. Some researchers [25] adopted reduced chemical kinetics rather than full kinetics to save computational burden. Speeding up the chemistry calculation approach, such as in situ adaptive tabulation (ISAT) [26,27], was applied in open space and then introduced into the simulation of porous media combustion. This approach was adopted by Yakovlev and Zambalov [13] to save computational time in modeling of

filtration combustion. A simplified theoretical solution of the LCL was presented by Shi et al. [28] using the analogy approach. They reported that an enormous computing time was saved with the procedure compared to the complete model. An RFB can also be used for syngas production. For predictions of full syngas components in an RFB, full chemical kinetics is necessary and this leads to enormous computational time [29,30].

A new approach to simulate combustion and heat recovery in an RFB was proposed by Yao and co-worker [31]; a steady state model was developed with one-step kinetics and the effect of extraction locations and the equivalence ratio on the heat extraction efficiency were studied. Their results indicated that computational time can be saved using their developed model, and multi-step chemical kinetics was recommended for the purpose of more accurate results.

Previous research on RFBs showed that the combustion characteristics of an RFB have been numerically studied based on the volume-averaged model with one-step kinetics. The predictions of the LCL with full chemical kinetics have rarely been used due to costly computation, this approach is very important to deeply understand the characteristics of the system and optimization design of the burner.

The objective of this work is to present a steady state model for the RFB system with full kinetics. This work makes the following contributions: (1) a steady state model with full chemical kinetics was developed using the analogy approach; (2) the developed model was validated against experimental data and predictions; (3) the combustion characteristics of an RFB at the LCL were analyzed, and the effects of heat loss and burner length on the LCL were predicted; and (4) the computational time using the developed and complete model for the same operating conditions was compared to evaluate the computational efficiency of the developed model.

2. Numerical Model

2.1. Geometry of the RFB

The RFB under study was used by Hoffmann and coworker [15], and the burner has a length of 0.2 m and was packed with ceramic foams for different pore sizes. All the used ceramic foams have the same porosity (ε) of 0.875. The burner was thermally insulated by Kaowool-board having a thickness of 92 mm. Tokyo city gas 13 A (88% methane, 5.8% ethane, 4.5% propane, and 1.7% butane; low heating value, 46,000 kJ/m^3) was used as fuel in the experiment [15]. For convenience, the mentioned gas was replaced with 100% methane. In this study, the LCL of an RFB with 13 ppi ceramics foam was numerically studied.

For the purpose of simplification, the following assumptions are used in the model:

(1) The gas flow in porous media is laminar and the working gas is non-radiating.
(2) The packing bed is inert and has an optical thickness, and the solid radiation is computed by the Rosseland assumption.
(3) Pressure drop in the packed bed is neglected.

The governing equations are obtained as follows [31]:

Continuity equation:

$$\frac{\partial(\varepsilon\rho_g)}{\partial t} + \frac{\partial(\varepsilon\rho_g u_g)}{\partial x} = 0 \quad (1)$$

where ε, t, x,ρ_g and u_g represent, respectively, the porosity, time, coordinate, gas density, and gas velocity.

Gas phase energy equation:

$$\varepsilon\frac{\partial}{\partial t}(\rho_g c_g T_g) - \varepsilon\frac{\partial}{\partial x}\left(\lambda_g\frac{\partial T_g}{\partial x}\right) + \varepsilon\frac{\partial}{\partial x}(\rho_g c_g u_g T_g) + h_v(T_g - T_s) + \varepsilon\sum_{i=1}^{n}\omega_i h_i W_i = 0 \quad (2)$$

The combustion of methane was modeled by the full kinetics GRI-Mech 3.0, and is composed of 53 species and 325 elementary reactions [32]. As recommended by Yao et al. [31], the full kinetics is used in this model for the purpose of more accurate results,

in addition to the prediction of pollutants of CO and NO for the future study. h_v is the volumetric heat transfer coefficient [33]:

$$h_v = Nu \times \lambda_g / d^2_{pore}, Nu_v = 0.819\left[1 - 7.33(d_{pore}/L)\right] \mathrm{Re}_v^{0.36[1+15.5(d_{pore}/L)]} \quad (3)$$

where d_{pore} is the pore size of porous media, L is the burner length.

Species conservation equation:

$$\frac{\partial}{\partial t}(\rho_g Y_i) + \frac{\partial}{\partial x}(\rho_g u_g Y_i) - \frac{\partial}{\partial x}\left(\rho_g D_i \frac{\partial Y_i}{\partial x}\right) - \omega_i W_i = 0 \quad (4)$$

Solid phase energy equation:

$$(1-\varepsilon)\rho_s c_s \frac{\partial T_s}{\partial t} = \frac{\partial}{\partial x}\left(\left[\lambda_{s,eff} + \lambda_{rad}\right]\frac{\partial T_s}{\partial x}\right) + h_v(T_s - T_g) - \beta(T_s - T_0) \quad (5)$$

where ρ_s, c_s are solid density and specific heat, and T_s and $\lambda_{s,eff}$ represent, respectively, solid phase temperature and the effective thermal conductivity of packing bed. β denotes the heat loss factor to the surroundings [30]. λ_{rad} is radiation conductivity and is computed as:

$$\lambda_{rad} = \frac{16}{3}\sigma\varepsilon_r d_{pore} {T_s}^3 \quad (6)$$

where σ is the Stefan–Boltzmann constant, ε_r is solid surface emissivity.

2.2. Steady State Model

In a previous study, Yao and Saveliev [31] presented a full analogy analysis of the steady state model for an RFB with heat extraction. However, in our model, the heat extraction is not considered and the full chemical kinetics is taken into account, and the porous media used in this study is different from that in Ref. [31]. For the convenience of the following description, the analogy processes for an RFB are conducted in this work.

Figure 1 shows the steady state model, including two parts separated by a highly conductive wall. The premixed methane/air mixtures are simultaneously sent into the porous burner by two flows in the opposite direction. The heat exchange occurs between the two flows through the highly conductive wall, and the temperatures in the two channels along the axis direction are same when the wall is highly conductive in the axis direction.

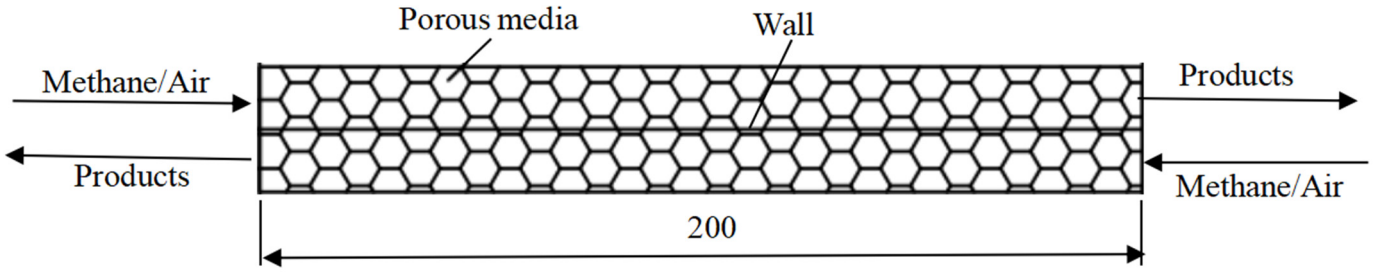

Figure 1. Time-averaged model.

The governing equations for the RFB:

Continuity equation:

$$\frac{\partial(\rho_g u_g)}{\partial x} = 0 \quad (7)$$

Gas phase energy equation:

$$-\varepsilon\frac{\partial}{\partial x}\left(\lambda_g \frac{\partial T_g}{\partial x}\right) + \varepsilon\frac{\partial}{\partial x}(\rho_g c_g u_g T_g) + h_v(T_g - T_s) + \varepsilon\sum_{i=1}^{n}\omega_i h_i W_i = 0 \quad (8)$$

Solid phase energy equation:

$$\frac{\partial}{\partial x}\left(\left[\lambda_{s,eff}+\lambda_{rad}\right]\frac{\partial T_s}{\partial x}\right)+h_v(T_s-T_g)-\beta(T_s-T_0)=0 \quad (9)$$

Species conservation equation:

$$\frac{\partial}{\partial x}(\rho_g u_g Y_i)-\frac{\partial}{\partial x}\left(\rho_g D_i\frac{\partial Y_i}{\partial x}\right)-\omega_i W_i=0 \quad (10)$$

2.3. Boundary Conditions, Initial Condition and Solution Process

The boundary conditions for the burner inlet and outlet are expressed as follows:

(1) Inlet:

$$T_g=300\text{K}, u_g=u_{g,0}, Y_{CH_4}=Y_{CH_4,in}, Y_{O_2}=Y_{O_2,in}$$

A pressure outlet is imposed at the burner outlet, and the non-slip condition at the wall is applied for the mixture velocity. The governing Equations (7)–(10) were calculated by CFD software Fluent 15.0. The SIMPLE method was used to treat the pressure field. To model the ignition process, the solid phase temperatures in the center of the RFB with length of 60 mm were specified to be 1600 K. The investigated ranges of equivalence ratio and mixture velocity are $0.022 \leq \phi \leq 0.091$, and $0.083\ \text{m/s} \leq u_{g,0} \leq 0.66\ \text{m/s}$, respectively. A uniform mesh of 0.5 mm was used in the calculation. The residual error of energy equation was 10^{-6}, and that of other equations was 10^{-3}. The symbols in this study are summarized in Nomenclature. The solid properties and parameters used in the computation are summarized in Table 1.

Table 1. Solid phase properties used in this work [15,20].

Pores per Inch	ε	d_{pore} (m)	ε_r	λ_s	β
#13	0.875	4.38×10^{-3}	0.8	1 W/m·K	80 W/m^3·K

3. Model Verification

To evaluate our model, the predicted temperatures and LCL for the RFB were compared with the experimental results [15] and predictions [20]. Figure 2 shows the predicted temperatures and experimental results [15]; the predictions by complete model with one-step kinetics [20] are also shown for comparison. The main parameters of the ceramic foam were taken from the experiment [15] and numerical work [20]: porosity ε = 0.875, pore size d_{pore} = 4.38 × 10^{-3} m for 13 ppi ceramics foam, surface emissivity of porous media ε_r = 0.8, λ_s = 1 W/m·K, and β = 80 W/m^3·K. It is noted that the gas and solid temperatures along the flow direction in the two channels are the same; this corresponds to the assumption made in the model. Thus, the predictions are shown along the flow direction of the one channel. As shown in Figure 2a, the predicted temperatures at both sides of the burner show reasonable agreement between the predicted temperatures and the experimental values. However, the maximum temperatures in the middle of the burner are under-predicted. The model fails to predict the temperatures at the middle of the reactor. It is noted that the heat loss through the burner walls to the surroundings in this study is taken into account by adding a source term to the solid energy equation. The heat loss flux is assumed to be the difference between the solid and ambient temperature, and the heat loss coefficient β is used in the empirical formula. This assumption is unrealistic for the practical burner and β is assumed to be constant in this work. This may lead to a huge error in modeling the temperature distributions in the burner and needs further study.

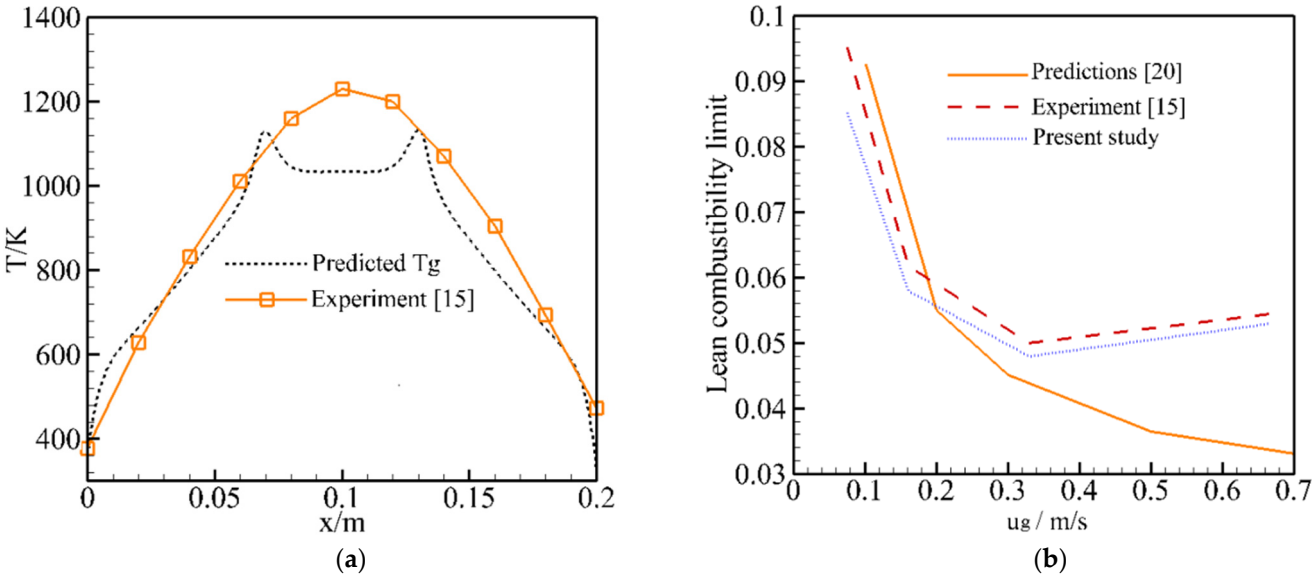

Figure 2. Predicted gas temperature and lean combustibility limit for the Reverse Flow Burner (β = 80 W/m^3·K). (**a**) Predicted T_g for equivalence ratio of 0.1, mixture velocity of 0.083 m/s and experimental results; (**b**) Predicted lean combustibility limit as a function of mixture velocity [15,20].

In this work, the LCL was determined by sequentially decreasing the equivalence ratio until flameout occurred. The steady state model was validated against an experiment [15] and the predictions [20] using a complete model with one-step kinetics, as shown in Figure 2b. A reasonable quantitative relationship between the simulations and the experiment can be observed, but our predictions are generally smaller than the results of the experiments. The predictions by Dobrego et al. [20] show the same trend as the experiment when the mixture velocity is smaller. However, an opposite trend is predicted by the one-step kinetics as the mixture inlet velocity is greater than 0.3 m/s. One can see that improved predictions are obtained by this model compared to the one-step kinetics model. The predicted LCL in Figure 3 is obtained based on the suggested β = 80 W/m^3·K. In the following we study the effect of β on the LCL.

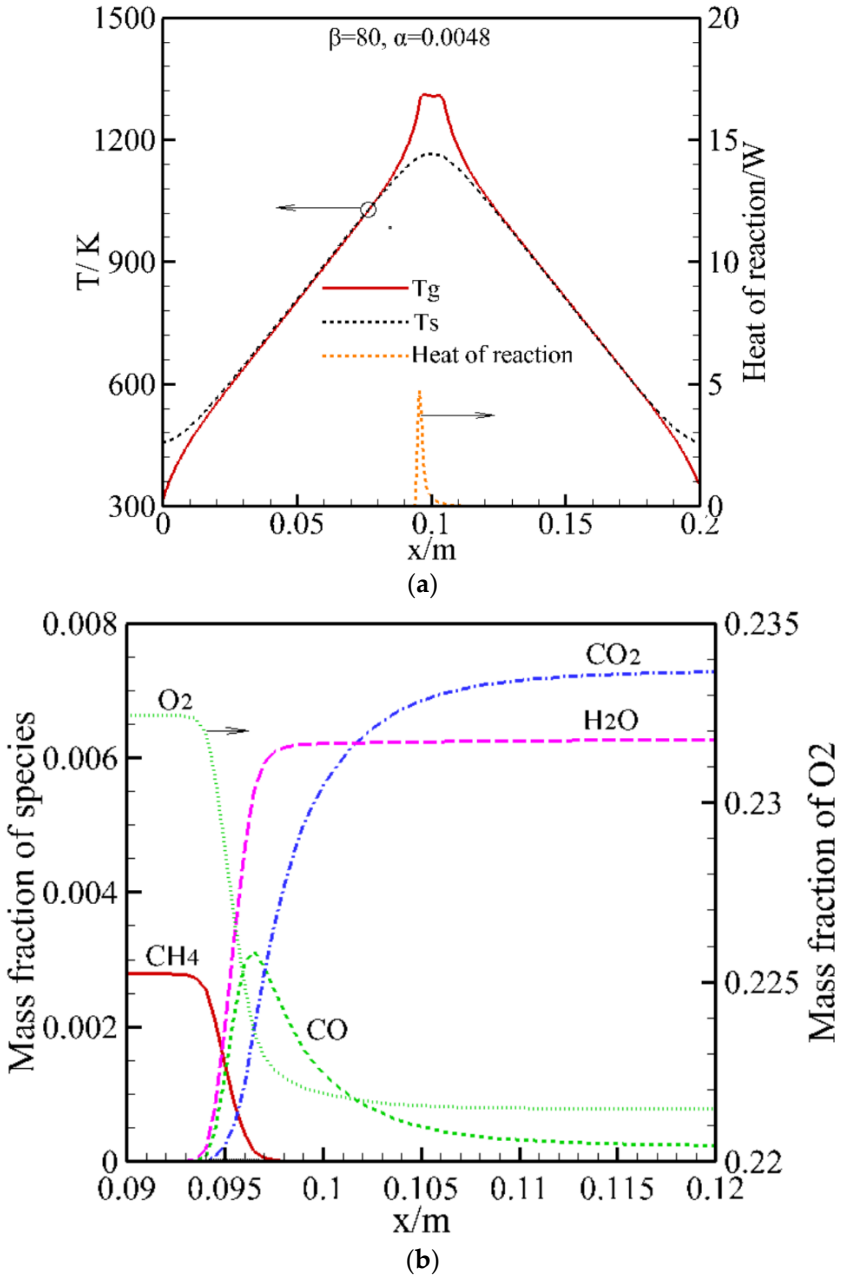

Figure 3. Numerically predicted temperature profile, heat of reaction and species near the flame zone for mixture velocity of 0.33 m/s and equivalence ratio of 0.0048. (**a**) Temperature profiles and heat of reaction; (**b**) Mass fraction of species.

4. Results and Discussions

4.1. Temperature and Species Distribution at LCL

To understand the typical characteristics of combustion near the flammability limit of the RFB at the steady state of the LCL, Figure 3 shows gas phase and solid temperatures, heat of reaction, and the main species near the flame zone for u_g = 0.33 m/s and ϕ = 0.0048 under the steady state of the LCL. A narrow high temperature zone located in the middle of the burner is observed in Figure 3a; this is a typical characteristic of an RFB when the RFB reaches its steady state at a lower equivalence ratio. Figure 3b shows an expanded view of the main species in the reaction zone. In this study the methane combustion was modeled with full chemical kinetics. It is shown in Figure 3b that CH_4 is pyrolyzed to intermediate hydrocarbons and then oxidized to CO; finally, CO is oxidized to CO_2 in a slow process. It is observed in Figure 3a that the heat release rapidly reaches its maximum

and then decreases slowly. This corresponds to the slow oxidation process of CO into CO_2. It is noted that CO oxidation to CO_2 is incomplete and CO emission may be high in the products. This incomplete conversion of CO to CO_2 leads to enormous CO emission in the RFB at the lower equivalence ratio. Although good performance regarding pollutant emission was reported in previous research, in this work enormous CO emission was predicted. This is an open problem that requires further study.

4.2. Effect of Heat Loss on Lean Combustibility Limit

Figure 4 shows the influence of heat loss on the LCL for different mixture velocities. The heat loss coefficient $\beta = 80$ W/m^3·K is recommended by Dobergo et al. [20], considering the insulation layer material and thickness used in the experiment. Our predictions show that the LCL can be extended by decreasing the heat loss coefficient. This may be explained by the fact that more heat is stored in the system when the heat loss coefficient is decreased. The value $\beta = 0$ corresponds to the adiabatic condition, which means that no heat loss occurs through burner walls to the surroundings. However, our results show that better agreement between the prediction and experiment was obtained for $\beta = 160$ W/m^3·K and $\beta = 320$ W/m^3·K, and the predicted LCL for $\beta = 160$ W/m^3·K and $\beta = 320$ W/m^3·K was slightly smaller and greater than the experimental results, respectively. The predictions [20] by the complete model with one-step kinetics are also shown for comparison. As shown in Figure 4, improved predictions of LCL are achieved by the present model compared to the results of Ref. [20], especially when the mixture velocity exceeds 0.2 m/s. The deviation between the present predictions and the experiment may be explained by multiple factors. The main reason may be the uncertainty of the thermal performance of the packed bed. Furthermore, it should be noted that the fuel in the experiment was replaced with methane, which may contribute to the deviation. As illustrated in Figure 4, heat loss has a significant influence on the LCL, and the inaccurate selection of β leads to the deviation between the prediction and the experiment.

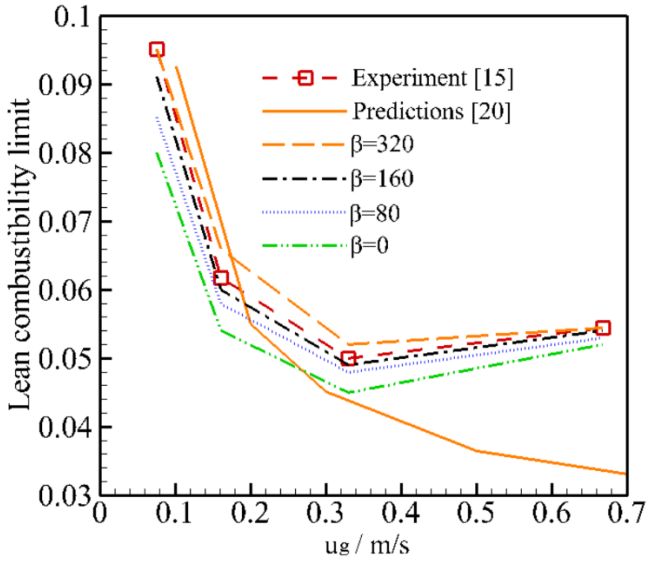

Figure 4. Effect of heat loss on the lean combustibility limit for different mixture velocities and 13 ppi ceramics foam [15,20].

4.3. Effect of Burner Length on Lean Combustibility Limit

In the experimental study by Hoffmann et al. [15], the LCL was finally extended from 0.028 to 0.026 for a natural gas/air mixture by increasing the burner length and cross section. In this work, the influence of burner lengths on LCL was evaluated; LCL curves as a function of mixture velocity for different burner lengths are shown in Figure 5. As shown in Figure 5, increasing the burner length extends the LCL. This is because more

heat can be stored in the system as the burner length is increased for the same operating conditions. It is noted that a long packing bed leads to an increase in the pressure drop and a large apparatus. However, porous media having a high porosity (0.875) were used in this study; thus, the pressure loss through the burner can be ignored. The convective heat transfer coefficient between two phases, and the properties, porosity, and pore size of the porous media may have significant effects on the LCL. However, these effects are beyond the scope of this study and need further investigation.

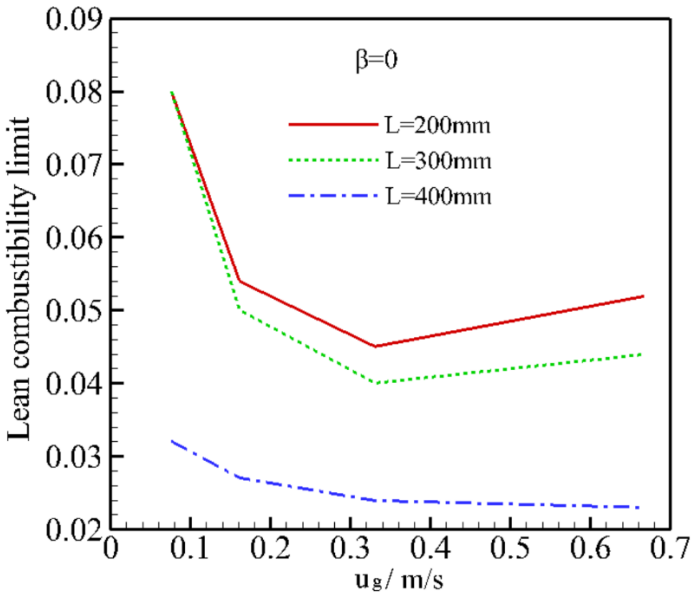

Figure 5. Lean combustibility limit as a function of the mixture velocity for different burner lengths.

4.4. Computational Time Comparison

We conducted a computational case study using the steady state model and complete model to evaluate the performance of the computational efficiency of the steady state model. The constant time step for the complete model was specified to be 1×10^{-5} s and the flow direction was changed automatically by a journal file compiled as a user-defined function. The computational case study was conducted by employing the same mesh, properties, and solution method. Test calculations were performed for $\varphi = 0.29$, $u_g = 0.083$ m/s, $L = 0.2$ m, and a half cycle of 30 s. For simplicity, the computational time rather than CPU time was used as an index to compare the calculation performance of the two models. The computation was conducted on a workstation with two CPUs (2.10 GHz) and 128 GB RAM. Our results show that computational times of 20 min and 31,200 min were required for the developed and complete models. This indicates that an enormous amount of time can be saved using the developed model, and the computational time can be reduced by 1560 times by applying the developed model compared to the complete model.

5. Conclusions

A steady state model for an RFB with full kinetics was developed based on analogy with a counter-flow reactor. It was confirmed that an improved prediction of the LCL was achieved by the developed model compared to the conventional transient model. Heat loss has a significant influence on the LCL; an increase in the heat loss leads to an increase in the LCL. By contrast, the LCL is decreased when the mixture velocity is increased, and the oppose trend is predicted by the present model. This indicates that computational time can be saved by a factor of 1560 when using the steady state model, which obtains accurate results compared to the complete model with one-step kinetics. The validated model can

be used for RFB design and optimization with accurate results and shorter computational time.

Author Contributions: Conceptualization, J.L. and J.S.; Methodology, M.M., X.K. and D.Z. All authors have read and agreed to the published version of the manuscript.

Funding: This work is supported by the National Natural Science Foundation of China (grant nos. 51876107, 52106170).

Institutional Review Board Statement: Not applicable.

Informed Consent Statement: Not applicable.

Data Availability Statement: Data are contained within the present article.

Acknowledgments: The author is grateful to many colleagues with whom he had the privilege to interact and collaborate over the years and whose work is partially referenced in this article.

Conflicts of Interest: We declare we have no competing interest.

Nomenclature

Abbreviations

c	specific heat, J/kg · K
D_i	diffusion coefficient of species i, cm^2/s
h_i	the molar enthalpy of species i, kJ/kg
T	temperature, K
u_g	gas mixture velocity, m/s
x	coordinate, m
d_{pore}	pore diameter of porous media, m
h_v	convective heat transfer coefficient, $W/m^3 \cdot K$
t	time, s
T_0	ambient temperature, K
W_i	molecular weight of species i, kg/kmol
Y	mass fraction

Greek symbols

φ	equivalent ratio
λ_{rad}	radiation conductivity, W/m · K
ρ	density, kg/m^3
ε_r	solid surface emissivity
β	heat loss coefficient, $W/m^3 \cdot K$
λ	thermal conductivity, W/m · K
$\lambda_{s,eff}$	thermal conductivity of packed bed, W/m · K
ε	porosity
ω_i	reaction rate of species i, $kmol/m^3 \cdot s$
σ	Stephan-Boltzmann constant, $W/m^2 \cdot K^4$

subscripts

G	gas
S	solid

References

1. Gosiewski, K.; Pawlaczyk, A.; Jaschik, M. Energy recovery from ventilation air methane via reverse-flow reactors. *Energy* **2015**, *92*, 13–23. [CrossRef]
2. U.S. EPA. U.S. Underground Coal Mine Ventilation Air Methane Exhaust Characterization. Coal mine ventilation air methane exhaust characterization. In *Coal Bed Methane Outreach Program*; U.S. EPA: Washington, DC, USA, 2010; pp. 1–16.
3. Mao, M.; Shi, J.; Liu, Y.; Gao, M.; Chen, Q. Experimental investigation on control of temperature asymmetry and nonuniformity in a pilot scale thermal flow reversal reactor. *Appl. Therm. Eng.* **2020**, *175*, 115375. [CrossRef]
4. Egerton, A.; Gugan, K.; Weinberg, F.J. The mechanism of smouldering in cigarettes. *Combust. Flame* **1963**, *7*, 37–73. [CrossRef]
5. Weinberg, F.J. Combustion temperature: The future? *Nature* **1971**, *233*, 239–241. [CrossRef] [PubMed]
6. Song, F.Q.; Wen, Z.; Dong, Z.Y.; Wang, E.Y.; Liu, X.L. Ultra-low calorific gas combustion in a gradually-varied porous burner with annular heat recirculation. *Energy* **2017**, *119*, 497–503. [CrossRef]

7. Banerjee, A.; Saveliev, A.V. High temperature heat extraction from counterflow porous burner. *Int. J Heat Mass Transf.* **2018**, *127*, 436–443. [CrossRef]
8. Liu, H.S.; Wu, D.; Xie, M.Z.; Liu, H.; Xu, Z.J. Experimental and numerical study on the lean premixed filtration combustion of propane/air in porous medium. *Appl. Therm. Eng.* **2019**, *150*, 445–455. [CrossRef]
9. Bubnovich, V.; Toledo, M. Analytical modelling of filtration combustion in inert porous media. *Appl. Therm. Eng.* **2007**, *27*, 1144–1149. [CrossRef]
10. Shi, J.R.; Xie, M.Z.; Liu, H.; Li, G.; Zhou, L. Numerical simulation and theoretical analysis of low-velocity filtration combustion of lean mixture. *Int. J. Heat Mass Trans.* **2008**, *51*, 1818–1829. [CrossRef]
11. Vahid, V.; Chanwoo, P. Analytical solutions of superadiabatic filtration combustion. *Int. J. Heat Mass Trans.* **2018**, *117*, 740–747.
12. Liu, C.; Pan, M.; Zheng, L.; Lin, P. Effects of heterogeneous catalysis in porous media on nanofluid-based Reactions. *Int. Commun. Heat Mass Transf.* **2020**, *110*, 104434. [CrossRef]
13. Yakovlev, I.; Zambalov, S. Three-dimensional pore-scale numerical simulation of methane-air combustion in inert porous media under the conditions of upstream and downstream combustion wave propagation through the media. *Combust. Flame* **2019**, *209*, 74–98. [CrossRef]
14. Jiang, L.S.; Liu, H.S.; Suo, S.Y.; Xie, M.Z.; Bai, M.L. Simulation of propane-air premixed combustion process in randomly packed beds. *Appl. Therm. Eng.* **2018**, *14*, 153–163. [CrossRef]
15. Hoffmann, J.G.; Echigom, R.; Yoshida, H.; Tada, S. Experimental study on combustion in porous media with a reciprocating flow system. *Combust. Flame* **1997**, *111*, 32–46. [CrossRef]
16. Barcellos, W.M.; Carlos, L.; Souza, E.O.; Saveliev, V.A.; Kennedy, L.A. Ultra-low-emission steam boiler constituted of reciprocal flow porous burner. *Exp. Therm. Fluid Sci.* **2011**, *35*, 570–580. [CrossRef]
17. Zeng, H.Y.; Wang, Y.Q.; Gong, S.Q.; Shi, Y.X.; Cai, N.S. Catalytically enhanced methane-rich combustion by porous media reactor. *Fuel* **2019**, *248*, 65–75. [CrossRef]
18. Oliveira, M.; Kaviany, M. Nonequilibrium in the transport of heat and mass reactants in combustion in porous media. *Prog. Energy Combust. Sci.* **2001**, *27*, 523–545. [CrossRef]
19. Hanamura, K.; Echigo, R.; Zhdanok, S.A. Superadiabatic combustion in a porous media. *Int. J. Heat Mass Trans.* **1993**, *36*, 3201–3209. [CrossRef]
20. Dobrego, K.V.; Gnesdilov, N.N.; Lee, S.H.; Chol, H.K. Lean combustibility limit of methane in reciprocal flow filtration combustion reactor. *Int. J. Heat Mass Trans.* **2008**, *51*, 2190–2198. [CrossRef]
21. Bubnovich, V.; Henríquez, L.; Díaz, C.; Maiza, M. Diameter of alumina balls effect on stabilization operation region for a reciprocal flow burner. *Int. J. Heat Mass Trans.* **2011**, *54*, 2026–2033. [CrossRef]
22. Henríquez-Vargas, L.; Valeria, M.; Bubnovich, V. Numerical study of lean combustibility limits extension in a reciprocal flow porous media burner for ethanol/air mixtures. *Int. J. Heat Mass Transf.* **2015**, *89*, 1155–1163. [CrossRef]
23. Vourliotakis, G.; Skevis, G.; Founti, M.A.; Al-Hamamre, Z.; Trimis, D. Detailed kinetic modelling of the T-POX reforming process using a reactor network approach. *Int. J. Hydrog. Energy* **2008**, *33*, 2816–2825. [CrossRef]
24. Shi, J.R.; Mao, M.M.; Li, H.L.; Liu, Y.Q.; Sun, Y.S. Pore-level study of syngas production from fuel-rich partial oxidation in a simplified two-Layer burner. *Front. Chem.* **2019**, *7*, 793–798. [CrossRef] [PubMed]
25. Dixon, A.G. Local transport and reaction rates in a fixed bed reactor tube: Endothermic steam methane reforming. *Chem. Eng. Sci.* **2017**, *168*, 156–177. [CrossRef]
26. Pope, S.B. Computationally efficient implementation of combustion chemistry using in situ adaptive tabulation. *Combust. Theor. Model.* **1997**, *1*, 41–63. [CrossRef]
27. Koren, C.; Vicquelin, R.; Gicquel, O. Self-adaptive coupling frequency for unsteady coupled conjugate heat transfer simulations. *Int. J. Therm. Sci.* **2017**, *118*, 340–354. [CrossRef]
28. Shi, J.R.; Xie, M.Z.; Li, G. Approximate solutions of lean premixed combustion in porous media with reciprocating flow. *Int. J. Heat Mass Trans.* **2009**, *52*, 702–708. [CrossRef]
29. Dobrego, K.V.; Gnezdilov, N.N.; Lee, S.H.; Choi, H.K. Partial oxidation of methane in a reverse flow porous media reactor: Water admixing optimization. *Int. J. Hydrog. Energy* **2008**, *33*, 5534–5544. [CrossRef]
30. Zheng, C.H.; Cheng, L.M.; Cen, K.F.; Bingue, J.P.; Savelieva, A. Partial oxidation of methane in a reciprocal flow porous burner with an external heat source. *Int. J. Hydrog. Energy* **2012**, *37*, 4119–4126. [CrossRef]
31. Yao, Z.X.; Saveliev, A.V. High efficiency high temperature heat extraction from porous media reciprocal flow burner: Time-averaged model. *Appl. Therm. Eng.* **2018**, *143*, 614–620. [CrossRef]
32. Bowman, C.T.; Hanson, R.K.; Davidson, D.F.; Gardiner, W.C.; Lissianski, J.V.; Smith, G.P.; Golden, D.M.; Frenklach, M.; Goldenberg, M. Available online: http://www.me.berkeley.edu/gri_mech/ (accessed on 5 July 1995).
33. Younis, L.B.; Viskanta, R. Experimental determination of the volumetric heat transfer coefficient between stream of air and ceramic foam. *Int. J. Heat Mass Trans.* **1993**, *36*, 1425–1434. [CrossRef]